IEEE Access
Multidisciplinary | Rapid Review | Open Access Journal

Received July 16, 2019, accepted July 26, 2019, date of publication August 12, 2019, date of current version August 26, 2019.

Digital Object Identifier 10.1109/ACCESS.2019.2934764

Fully Integrated Liquid-Core Waveguide Fluorescence Lifetime Detection Microsystem for DNA Biosensing

LIPING WEI[1], HOI MAN LEUNG[2], YI TIAN[1], PIK KWAN LO[2], AND DEREK HO[1], (Member, IEEE)

[1]Department of Materials Science and Engineering, City University of Hong Kong, Hong Kong
[2]Department of Chemistry, City University of Hong Kong, Hong Kong

Corresponding author: Derek Ho (derekho@cityu.edu.hk)

This work was supported in part by the Hong Kong Research Grants Council under Project 11213515.

ABSTRACT Time-resolved fluorescence is a widely adopted technique for DNA detection due to its high sensitivity and selectivity. However, due to stringent requirements on optics and electronics, instrumentation with time-resolved capability is bulky and expensive, prohibiting their use in portable and point-of-care applications. In this work, a fully-integrated DNA biosensor based on liquid-core waveguide (LCW) optics for fluorescence lifetime analysis is presented. The DNA biosensor encompasses all-custom bioassay, optics and electronics into a microsystem, delivering a near sample-to-answer level of integration. Lifetime, rather than intensity, is exploited as the analytical signal from the V-carbazole probe for the first time. Excitation propagation within the LCW is investigated both analytically and in simulations to achieve high excitation rejection and low temporal dispersion, enabling the proposed LCW-based system with much smaller instrumentation size to deliver comparable lifetime measurement accuracy to traditional systems. Detection of DNA down to 15 base pairs at a low detection limit of 1.38 nM demonstrates the high applicability of the proposed biosensor for compact, application-specific, and low-cost diagnostics devices.

INDEX TERMS DNA biosensing, fluorescence lifetime detection, liquid-core waveguide, TCSPC, turn-on fluorescent probe.

I. INTRODUCTION

Demand for accurate, rapid, and low-cost medical diagnostics is rising on a global scale. Medical diagnostics has wide applications from viral and pathogenic screening to genetic and cancer studies. At the core of medical diagnostics is the detection and analysis of biomolecules such as deoxyribonucleic acid (DNA) and protein [1]–[3].

Recently, there has been several investigations of DNA nanotechnology, utilizing self-assembled DNA 3D nanostructures that are small in size (<100 nm), nontoxic, and stable for carrying therapeutic agents or drugs to specific type of cells and organelles [4], [5]. The method of using highly selective fluorescent probes to monitor DNA hybridization (or the reverse process) provides spatial and temporal feedback, significantly improving the precision of, for example, drug delivery, which is illustrated in FIGURE 1. FIGURE 1(a) depicts a molecular complex consisting a double stranded DNA (dsDNA), a turn-on fluorescent probe, and a drug to be delivered. The probe, which operates based on the turn-on effect, show significant fluorescence as it is bound to DNA initially [6]. Due to enzymatic digestion in target organelles, as shown in FIGURE 1 (b), the dsDNA unwinds and splits into pieces, which results in the detachment of the probe and drug [7]. Once detached from the dsDNA, the probe turns off. Therefore, the turn off event of the fluorescent probe indicates that dsDNA has become single-stranded DNA (ssDNA) and the drug is also detached from the complex, thus providing accurate feedback that the drugs are delivered successfully.

DNA sensing based on fluorescence lifetime measurement (FLM) has attracted substantial interests recently, due to many intrinsic advantages, for instance, the signal being independent of probe concentration and excitation intensity,

The associate editor coordinating the review of this article and approving it for publication was Chunsheng Zhu.

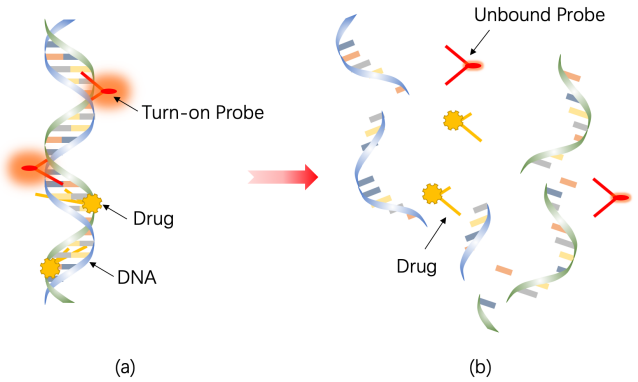

FIGURE 1. **Probe-assisted drug delivery and release process. (a) The complex of drug, DNA, and turn-on fluorescent probe. (b) Target release of drugs upon DNA unwinding, which can be monitored by detecting the turn-off event.**

as well as the ability to distinguish static and dynamic quenching [8]. Especially, signal independence on probe concentration is an advantage because when labeled cells are observed in a fluorescence microscope, the local concentration of the probe in each part of the cell is unknown. In addition, the probe concentration can vary due to photobleaching during the measurement. Therefore, lifetime measurement provides more accurate quantitative analysis. However, there are still challenges to fluorescence lifetime measurements, such as self-absorption in fluorescent samples, lack of accuracy provided by lifetime extraction algorithms, and bulkiness of the instrumentation. The main focus of this work is in the aspect of instrumentation.

Among FLM methods, a widely-adopted technique is time-correlated single-photon counting (TCSPC). Conventional bench-top fluorescence lifetime measurement equipment based on TCSPC technique has a low level of integration, rendering them bulky and expensive, thus unsuitable for wide in-field or point-of-care applications, where compact and automated devices are required. To circumvent the above limitations, a new breed of miniaturized sensors is enabled by a high level of integration into a microsystem. Sensor miniaturization has the advantages of reduced sample size, reaction time, sensor form-factor, power consumption, as well as cost. In the miniaturization of TCSPC instruments through design optimization, reduction in complexity and size of electronic components has been largely achieved primarily with complementary metal-oxide-semiconductor (CMOS) technology [9]–[11].

However, progress towards the optical subsystem has been limited. In a compact optical system, e.g. employing contact imaging, the fluorescent sample is typically placed in close proximity to the sensor surface as well as the excitation source [12]. The main challenge, as is well-known, lies in providing effective excitation rejection, in order to achieve high signal-to-noise ratio via minimizing the background. Excitation rejection is not a main challenge in conventional lifetime measurement systems, whereas it is particularly a problem for the design of compact instrument. Also, it is desirable to achieve the above through a single, compact optical component while maintaining single photon detection sensitivity.

A variety of techniques have been proposed for excitation rejection in fluorescence biosensors. Thin-film interference filters have been used to reject collimated excitation. Micro lenses have been used to focus excitation or emission [13]. Micro prisms have been used to divert excitation away from the detector [14], [15]. Cross-polarizers have been employed to filter excitation [16]. Micro waveguides have been used to separately propagate excitation and emission [17], [18].

In recent years, the liquid-core waveguide (LCW) has attracted substantial interests [19]–[22]. The LCW enables strong interaction between the excitation and the sample under analysis, thereby allowing high-sensitivity fluorescence detection with reduction in sample volume. With design optimization, the LCW has large potential to perform efficient excitation rejection while doubling up for sample holding, all by a single component. This unique advantage offers vast potential for the development of low-cost microsystems for fluorescence detection. In the last several years, optofluidic platforms based on the LCW have been investigated for different applications, such as for low concentration toxic gases detection [19], [23], real-time single molecule detection [24], flowing micro droplet based absorbance detection [18], and single-virus detection [17], [25].

However, despite its advantages, the LCW has not been exploited in FLM systems. One main engineering hurdle is the fact that when the excitation ray travels along the LCW, the excitation is decomposed into multiple split rays due to partial reflection, with split rays having different propagation path lengths, thus different propagation times. This has two main implications: (i) Different propagation time causes a fluorescent molecule at a particular spatial location to be excited by a dispersed excitation profile through time. (ii) Excitation takes more time to reach samples at the opposite end of the LCW. Overall, the time delay among the excitation split rays gives rise to temporal dispersion [26, p. 326], which affects the measurement of photon arrival time, thus deteriorating lifetime measurement accuracy. Therefore, the design of LCW TCSPC based FLM sensors to provide high excitation rejection and high temporal resolution remains a challenge.

In this work, a fully-integrated DNA biosensor based on liquid-core waveguide (LCW) optics for fluorescence lifetime analysis is presented. The DNA biosensor encompasses all-custom bioassay, optics and electronics into a microsystem, delivering a near sample-to-answer level of integration. The turn-on fluorescent probe, V-carbazole, is exploited as fluorescent lifetime probe for the first time. A design optimization technique is devised based on theoretical analysis and simulation to achieve high excitation rejection and low temporal dispersion for the LCW structure. A prototype LCW DNA biosensor microsystem is realized, demonstrating DNA detection down to 15 base pairs. The biosensor achieves a detection limit of 1.38 nM, elucidating the potential of

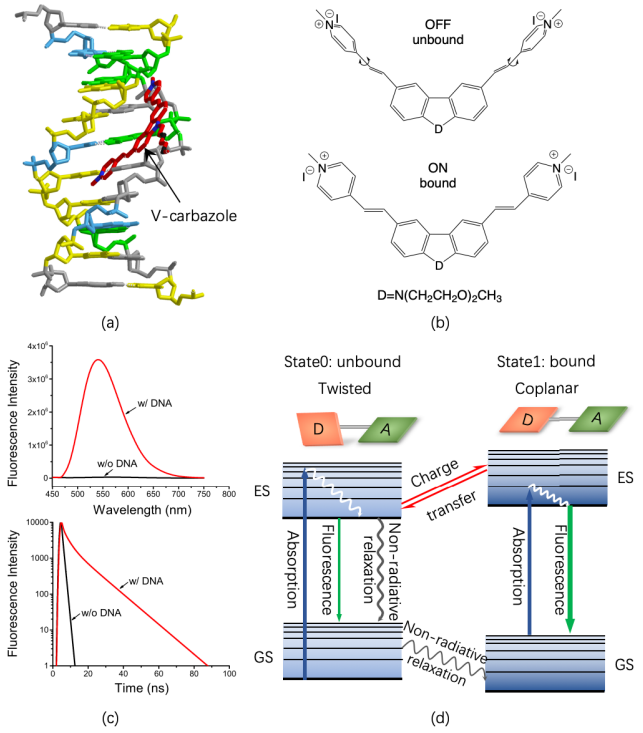

FIGURE 2. (a) Structure of the V-carbazole fluorescent probe, conjugated with DNA. (b) OFF state of the probe when unbound to DNA (top), ON state when bound to DNA (bottom). (c) Emission spectra (top) and decays (bottom) of the probe unbound and bound to DNA. (d) Jablonski diagrams of the probe unbound to DNA (twisted) and bound to DNA (coplanar), respectively. The white wavy lines represent vibrational relaxation. ES = excited electronic state, GS = ground electronic state, D-A = electron- donating and accepting groups. The two states result in two lifetime components.

the proposed LCW DNA biosensor for application-specific, low-cost, and compact time-resolved diagnostics.

II. DNA DETECTION CHEMISTRY

A. TURN-ON EFFECT

The detection scheme of DNA based on the turn-on effect is depicted in FIGURE 2. The turn-on effect is a mechanism by which, upon the hybridization of probe and DNA, the fluorescent probe turns from the OFF state (weak emission) to the ON state (strong emission). The turn-on fluorescent probe used in this work is a custom carbazole-based biscyanine with a bichromophoric skeleton, V-carbazole.

The V-carbazole molecule has been synthesized with a well-defined (minor groove) binding mode, suitable for the quantification of DNA. As the V-carbazole molecules are highly soluble in aqueous solution with no aggregation, they have been accurately modelled by the classical Beer-Lambert law up to a concentration of 0.1 mM. The absorption peak is approximately 455 nm, whereas emission ranges from 475 nm to 675 nm, i.e. with no significant overlap between the excitation and emission spectra. The broad absorption and emission bands in the visible range of V-carbazole diluted in a phosphate buffer can be attributed to the incorporation of the donor-acceptor-donor π-π^* system. FIGURE 1 (a) shows the concave shape and the positively charged recognition units at the end of each arm, enabling the V-carbazole to bind to DNA within the minor groove. Originally designed for two-photon excited fluorescence imaging, our previous work utilized the V-carbazole primarily as an intensity probe [27]. The capability of V-carbazole as a lifetime probe (as opposed to an intensity probe) for DNA detection is herein explored for the first time.

The rotation of the two arms of V-carbazole molecule controls optical switching as shown in FIGURE 2 (b). When the molecules are unbound to DNA, the two arms can freely rotate, and the excited electrons can readily dissipate their excess energy rapidly to the solvent non-radiatively, resulting in a weak fluorescence signal, which corresponds to the OFF state. Upon binding to DNA, the rotation of the two arms is restricted, thus more excited electrons can return to the ground state radiatively, resulting in enhanced fluorescence signal, which corresponds to the ON state. According to the definition of quantum yield and lifetime, as nonradiative rate decreases, both quantum yield and lifetime increase [8]. Accordingly, fluorescence intensity, which is proportional to quantum yield, has an inverse relationship with respect to nonradiative rate. Therefore, both the fluorescence intensity and lifetime can serve as analytical signals to be detected, as shown in FIGURE 2 (c).

The rotational freedom of the two arms of V-carbazole molecules contributes to a twisted structure of the molecules, whereas restricted rotation results in a coplanar conformation of the molecules. The transition between twisted conformation and coplanar conformation is caused by electron transfer, which is accompanied by intramolecular D–A (D and A refer to electron donating and accepting groups, respectively) twisting around the single bond [28]. The Jablonski diagram of these two states are depicted in FIGURE 2 (d). Upon binding to DNA, the reduced rotational freedom of the two arms of the coplanar conformation contributes to new energy levels with higher excited-state energy and lower ground-state energy [29]. The balance between twisted conformation and coplanar conformation often results in dual fluorescence, giving rise to two fluorescence lifetime components, which can be observed in subsequent results.

B. SAMPLE PREPARATION

The sequence of the DNA sample utilized in the detection measurement is as follows:

15-mer DNA: 5'-CTG AGA CTG GAA TGA-3'

15-mer complimentary DNA: 5'-TCA TTC CAG TCT CAG-3'

This sequence has been successfully applied in the lipid-functionalized DNA nanocages for drug delivery applications. The DNA strands were synthesized by standard automated oligonucleotide solid-phase synthesis (BioAutomation MerMade MM6 DNA synthesizer) [7]. The DNA strands were mixed in 80 μM of phosphate buffer with pH 7, subsequently heated to 60 °C and cooled to 4 °C for 4 hours by a thermal cycler. The detailed preparation process of V-carbaozle was presented in our previous work [27].

To tradeoff between sensitivity and dynamic range in DNA detection, the concentration of V-carbazole diluted in a pH 7 phosphate buffer solution was chosen to be 0.6 μM. Then, V-carbazole at 60 μM was added to the DNA samples to yield a final concentration of 0.6 μM of V-carbazole and a variety concentrations of DNA sample. The samples were stored at 4° C for subsequent usage.

III. LCW-TCSPC MICROSYSTEM

A. LCW

Excellent excitation rejection performance of the LCW can be achieved by detecting the emission perpendicular to the LCW because the excitation is well confined within the LCW, whereas the emission can exit the LCW. The confinement of the excitation is realized by total internal reflection (TIR) at the outer interface where the wall has a higher refractive index than the surrounding air. At the inner interface of an LCW, as the liquid core has a lower refractive index than the wall, only partial reflection occurs. At each partial reflection site, part of the light is reflected, and the remainder is refracted. After several iterations of partial reflections, the initially single excitation ray becomes multiple split rays, resulting in multipath propagation within the LCW.

Since different split rays have different propagation time due to the different propagation path lengths, a fluorescent molecule can be regarded as being excited at multiple instances through time. Moreover, excitation takes more time to reach samples further along the LCW. The time delay among the excitation split rays gives rise to temporal dispersion, which affects the measurement of photon arrival time, thus deteriorating lifetime measurement accuracy.

The temporal dispersion in an LCW is a function of the divergence angle, α, of the excitation beam and the propagation length, l, along the LCW. As l is a key design parameter, the effect of the divergence angle of the excitation beam is considered negligible in subsequent analysis. Subsequently, the temporal dispersion as a function of l is investigated. Detailed theoretical analysis is presented in the previous work [30].

To minimize the effect of temporal dispersion on the fluorescence lifetime measurement accuracy, the temporal dispersion should be designed to be smaller than the full width at half maximum (FWHM) of the single photon detector transit time spread (TTS) [31]. According to the multipath propagation model, temporal dispersion is reduced with respect to l. However, with a smaller l, less excitation photons are absorbed, generating less emission photons and resulting in weaker detectable emission intensity. Therefore, the ratio of the emission to the scattered excitation reaching the detector, i.e., the emission-to-excitation ratio, is reduced. Fluorescence decays with different emission-to-excitation ratios can be simulated using Monte Carlo method [32]. Lifetime values extracted from the simulated fluorescence decays for a series of propagation lengths and concentrations, i.e., for different emission-to-excitation ratios, are shown in FIGURE 3. It is

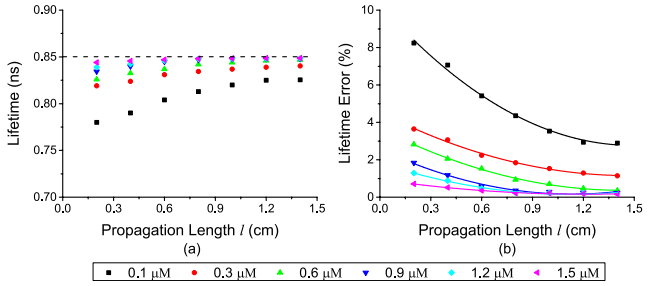

FIGURE 3. (a) Lifetime values extracted from the simulated fluorescence decays for a series of propagation lengths and concentrations (i.e. with different emission-to-excitation ratios). (b) Lifetime errors compared with the ideal value. The accuracy of the lifetime increases with increased propagation length and concentration.

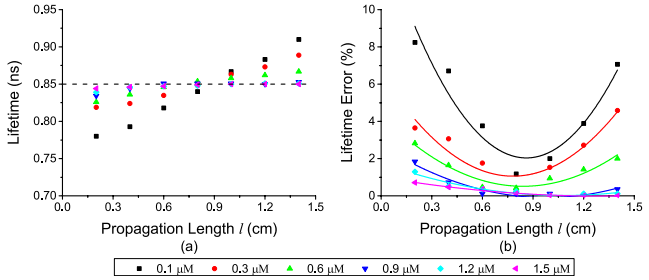

FIGURE 4. (a) Lifetime extracted from simulated fluorescence decays modeling the effect of temporal dispersion. (b) Lifetime errors (i.e., with respect to the theoretical value of 0.85 ns), showing an optimal region at moderate propagation length.

evident that a low emission-to-excitation ratio can lead to the deterioration of the lifetime measurement accuracy.

As a result, the choice of l involves a design tradeoff between achieving a low temporal dispersion and maintaining high emission-to-excitation ratio. Considering both temporal dispersion and emission-to-excitation ratio in the Monte Carlo simulation model, a region within the LCW defined by an optimal l can be determined, as shown in FIGURE 4.

Simulation was performed with the molar absorptivity of V-carbazole of 5.81×10^4 M^{-1} cm^{-1} and quantum yield of 0.0029. The wall thickness and inner diameter of the LCW are set to 0.8 mm and 6.4 mm, respectively. As evident from FIGURE 4, when l is small, lifetime error is dominated by the low emission-to-excitation ratio. When l is large, lifetime error is dominated by temporal dispersion. Therefore, an optimal region exists in the middle, ranging from 0.4 cm to 1.2 cm, where the lifetime error for V-carbazole concentrations above 0.3 μM is within 3%.

B. INTEGRATED LCW-TCSPC IMPLEMENTATION

The proposed integrated LCW DNA biosensor is shown as FIGURE 5. The sensor consists of a pulsed blue light source (nanoLED-455, Horiba) with pulse duration of 1.3 ns and repetition rate of 1 MHz as excitation, a thin-film neutral density (ND) filter (ND-LCD 10%, FUJIFILM) to attenuate excitation power (to prevent pile-up), a thin-film long-pass filter with optical density (OD) of five (e.g., 10^5 attenuation) to further reduce the residual excitation photons reaching the detector (only used in a subset of tests), an LCW for guiding

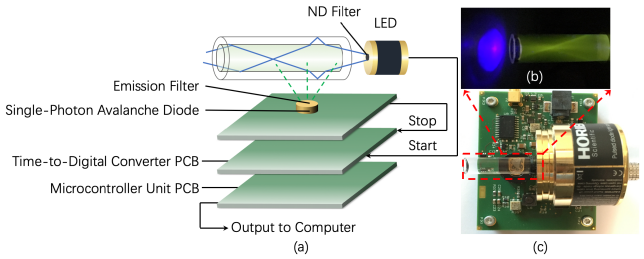

FIGURE 5. Implementation of the integrated LCW DNA biosensor: (a) schematic, (b) photograph of the LCW filled with fluorescent sample, and (c) top view of the integrated biosensor system.

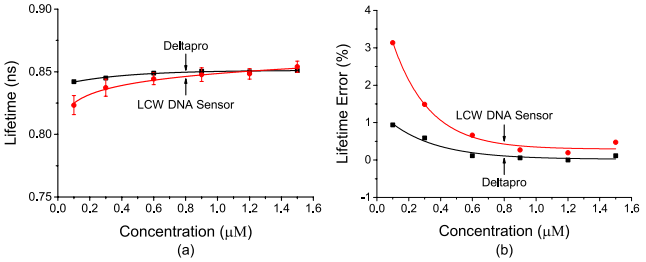

FIGURE 6. (a) Lifetime values measured by the proposed integrated LCW DNA biosensor and the commercially available Deltapro (as a comparison). The propagation length of the LCW is designed to be 0.8 cm (found to be optimal by simulation). (b) Lifetime errors.

the excitation and holding the sample solution, a single-photon avalanche diode (SPAD) (id101-50, IDQ), a time-to-digital converter (TDC) (TDC7200, Texas Instruments) with 55 ps temporal resolution for signal conversion, a microcontroller unit (MCU) (MSP430F5529, Texas Instruments) for data processing and control, and a custom-designed analog signal conditioning circuit. For controlling the propagation length, the tail end of the LCW is selectively covered with black tape. Therefore, it is not necessary to use LCWs of different lengths.

To make the SPAD operating in the Geiger mode, the diode anode is biased with a negative voltage, −26V, and the diode cathode is linked to a positive voltage, +5V, through a polysilicon resistor. The SPAD is operated when the temperature is below 70°C. With 45 ns deadtime, 100 Hz dark count rate, and 40 ps temporal resolution, the proposed SPAD is suitable for TCSPC-based fluorescence lifetime measurements.

The signal conditioning circuit with Texas Instruments LSF0102 two-channel bidirectional multi-voltage translator is customized to adjust the output signals of the excitation source and the SPAD to be compatible with the input requirement of the TDC.

IV. SYSTEM VALIDATION

A. PERFORMANCE OF THE TCSPC ELECTRONICS

The performance of the proposed TCSPC electronics can be characterized by the differential non-linearity (DNL), which is assessed by the code density test [33], [34]. In this test, two pulse generators produce two uncorrelated signals that represent START signal with a random rate and STOP signal with a fixed rate, respectively. To have a reasonably flat START-STOP input signal distribution, 3×10^4 time-to-digital conversion results per histogram bin are recorded, realizing a negligible statistical noise of signal distribution of 0.6%. The measured DNL of the proposed TCSPC electronics ranges between +9.7% and −8.5% of the least significant bit (LSB), with an average root mean square (RMS) value of 7% of LSB within a 500 ns full-scale range (FSR). Therefore, the proposed TCSPC electronics is capable of providing high-accuracy lifetime measurement.

B. SYSTEM VALIDATION USING V-CARBAZOLE

The proposed LCW DNA biosensor is characterized through lifetime measurements from the V-carbazole. The results from the proposed biosensor is compared with a commercially available FLM system (Deltapro, Horiba), as shown in FIGURE 6. The propagation length of the LCW is set to be 0.8 cm, which is within the optimal region. The V-carbazole diluted in a pH 7 phosphate buffer solution across a variety of concentrations is prepared. For Deltapro, V-carbazole solution is held in a standard quartz cuvette.

From FIGURE 6, it is evident that the lifetime error is rather large at concentrations below 0.1 μM, due to the weak fluorescence intensity. Although Deltapro outperforms the proposed biosensor slightly, Deltapro is a bench-top setup with significantly higher size, weight, and cost. This demonstrates that, through design optimization of excitation reject and temporal dispersion from the LCW, highly accurate fluorescence lifetime can be realized by a compact, integrated implementation.

C. SYSTEM VALIDATION IN DNA DETECTION

After performance characterization through lifetime measurements from the V-carbazole fluorophore, the proposed LCW DNA biosensor is verified through DNA detection. To evaluate the applicability towards practical DNA detection, lifetime measurements obtained from the proposed biosensor is compared with Deltapro. Both the fluorescence decays and the extracted lifetime have been analyzed. Sensor dynamic ranges under both lifetime- and intensity-medicated biosensing are compared. Detection limit of the proposed system is also analyzed.

1) FLUORESCENCE DECAYS

The fluorescence decays of V-carbazole when attached to DNA of a variety of concentrations are shown in FIGURE 7. FIGURE 7 (a) depicts the decays measured by the proposed sensor. As a reference, FIGURE 7 (b) depicts the decays measured by Deltapro. For comparison, the decays obtained by the proposed sensor and Deltapro are plotted together, for 25 nM and 100 nM of DNA, as shown in FIGURE 7 (c) and (d), respectively. It is evident that the proposed sensor performs similarly to Deltapro, which is far large in size and has a much high component count. Also, evident from FIGURE 7, fluorescence attenuates slower at higher DNA concentrations. This is because, with an increased DNA concentration, a larger number of

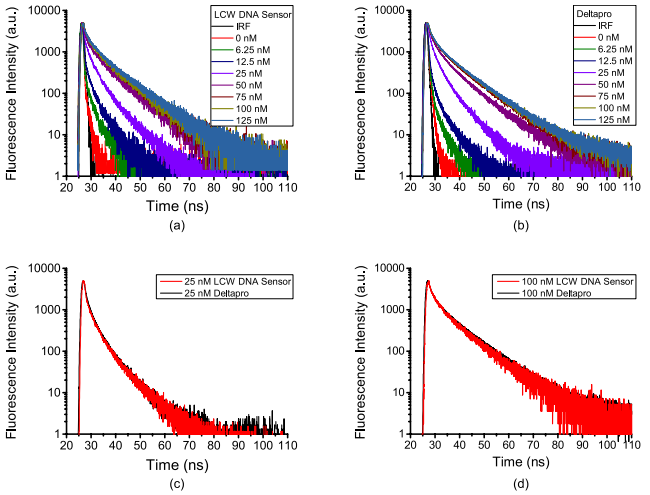

FIGURE 7. **Fluorescence decays of the V-carbazole probe across DNA concentrations. (a) and (b) show fluorescence decays across DNA concentrations obtained by the LCW DNA biosensor and Deltapro, respectively. (c) and (d) compare the decays obtained by the two systems of 25 nM DNA and 100 nM DNA, respectively. IRF is the instrumental response function of the entire system.**

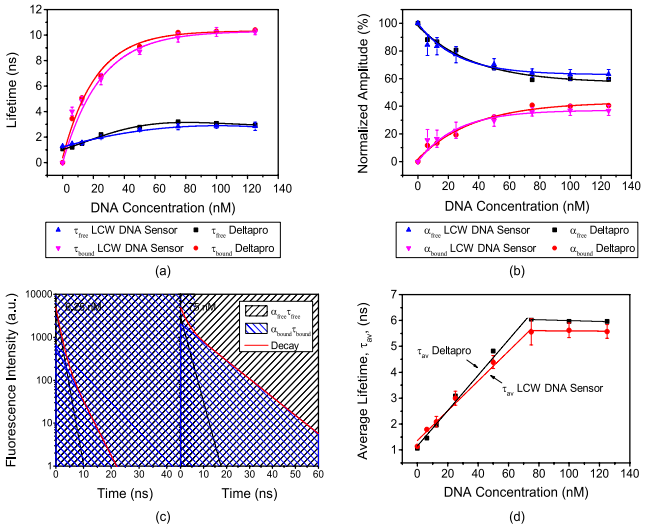

FIGURE 8. **(a) Lifetime components extracted from the decays measured by the LCW DNA biosensor and Deltapro. (b) Normalized amplitudes (showing percentage contribution) of two lifetime components for the LCW DNA biosensor and Deltapro. (c) Bi-exponential decays and corresponding mono-exponential components of the fluorescence decays for 6.25 nM and 75 nM of DNA. (d) Average lifetime across DNA concentrations. Linear region occurs for the DNA concentration range between 6.25 nM and 75 nM.**

DNA molecules are available to bind with the V-carbazole molecules, resulting in more V-carbazole molecules that are turned on, hence an increase in lifetime (and fluorescence intensity).

2) LIFETIME CHARACTERISTICS

Lifetime extraction from the fluorescence decays from both the proposed sensor and Deltapro was conducted using a decay analysis software (DAS6, Horiba) with results shown in FIGURE 8. For each DNA concentration, a total of three measurements were taken. Data from the proposed sensor and Deltapro are shown with standard deviations (plotted using error bars) and the average values, respectively. Results obtained by the proposed sensor and Deltapro correlate well with each other. As the cuvette used in Deltapro contains several times the sample volume compared to the LCW, which yields a much strong initial signal to be detected. Accounting for the sample volume difference, results further point towards the high performance of the proposed biosensor.

FIGURE 8 (a) and (b) exhibits the expected results of the fluorescence lifetime across DNA concentrations. Firstly, the decays can be well fitted onto a bi-exponential decay model, given by equation (1). The two components from the bi-exponential decay model represent V-carbazole molecules that are free in the solution and those that are bound to the DNA. The shorter lifetime component, τ_{free}, is contributed by the free V-carbazole molecules, whereas the longer lifetime component, τ_{bound}, is contributed by those bound to the DNA. Secondly, τ_{bound} dramatically increases with higher DNA concentration, whereas τ_{free} changes only slightly. According to the turn-on principle, upon binding to DNA, the rotation of V-carbazole molecules is restricted, resulting in a reduction in the non-radiative rate, hence a large increase in the lifetime. In addition, V-carbazole molecules are positively charged but DNA molecules are negatively charged. Therefore, the presence of DNA in the solution changes the local chemical environment of the V-carbazole molecules, thereby modulating the lifetime of the free V-carbazole molecules. Thirdly, the normalized amplitudes for each lifetime component as given by equations (2) and (3) have opposite trend. The normalized amplitudes provide information on the relative concentrations of emitting species, i.e., the unbound and bound V-carbazole molecules. The concentration of V-carbazole is fixed. With a higher DNA concentration, more V-carbazole molecules are bound to the DNA, reducing free V-carbazole molecules. The real fluorescence decay F(t), normalized amplitude corresponding to unbound V-carbazole molecules, α_{free}, and normalized amplitude corresponding to bound V-carbazole molecules, α_{bound}, are given by

$$F(t) = A + b_{free}e^{\frac{-t}{\tau_{free}}} + b_{bound}e^{\frac{-t}{\tau_{bound}}} \tag{1}$$

$$\alpha_{free} = \frac{b_{free}}{b_{free} + b_{bound}} \tag{2}$$

$$\alpha_{bound} = \frac{b_{bound}}{b_{free} + b_{bound}} \tag{3}$$

For multi-exponential decays, a more convenient means to observe the overall change of the fluorescence signal is via the average lifetime, τ_{av}, given by

$$\tau_{av} = \sum \alpha_i \tau_i \tag{4}$$

where the fractional intensity $\alpha_i\tau_i$, corresponding to the integral of $\alpha_i \exp(-t/\tau_i)$ with respect to time, represents the photon count contributed by the bound and unbound V-carbazole molecule with lifetime τ_i.

FIGURE 8 (c) presents the bi-exponential decays and the corresponding mono-exponential components. FIGURE 8(d) shows the average lifetime across the DNA concentration

TABLE 1. Comparison of the fluorescence lifetime dynamic range of this work with those reported in the literatures for DNA detection.

Probe name[a]	Lifetime range (ns)	Multiple	Refs
HEX	3.5~4.2 [b]	1.2	[35]
S-carbazole	1.95~2.37	1.22	[27]
ATTO 488	3.1~4.16	1.35	[36]
CdSe/ZnS	6.77~10.3	1.48	[37]
Rhodamine Green 110	2.59~4.08	1.58	[38]
Alexa 647	1.08~1.8	1.67	[36]
Doxorubicin	1.05~1.81 [b]	1.72	[39]
DRAQ5	0.23~0.5	2.17	[36]
Cy3	0.53~1.22 [b]	2.28	[40]
Nanoflare	0.46~1.23 [b]	2.64	[41]
M3HFaa	1.59~4.56 [b]	2.87	[42]
Cy3	0.18~0.52 [b]	2.89	[43]
FAM	0.59~2.14 [b]	3.62	[44]
dC^{bdp}	0.5~2.2 [b]	4.4	[45]
V-thiophene	0.48~2.18	4.54	[27]
V-carbazole	1~6.05 [b]	6.05	This work
Hoechst33258	0.3~3.5	11.67	[46]
RD2	0.07~1.22 [b]	17.43	[47]

[a] The probe name used in the literature.
[b] The corresponding lifetime is average lifetime.

ranging from 6.25 nM to 125 nM for both the LCW DNA biosensor and Deltapro. It is evident that the area $\alpha_{\text{bound}}\tau_{\text{bound}}$ (shaded blue) increases dramatically with DNA concentration, whereas the area $\alpha_{\text{free}}\tau_{\text{free}}$ (shaded black) has a slight increase, which shows the bound V-carbazole molecules with longer lifetime contribute most to the overall fluorescence signal. When the DNA concentration ranges from 6.25 nM to 75 nM, the average lifetime exhibits a linear response in the range of 1ns to 6.05ns. This six fold lifetime modulation provides a wide dynamic range for the biosensor. TABLE 1 shows a comparison of the fluorescence lifetime dynamic range of this work with those reported in the literature, elucidating the excellent suitability of the proposed bioassay for DNA detection. When the DNA concentration is increased beyond 75 nM, the average lifetime saturates to 6.05 ns. This is because the V-carbazole concentration is fixed at 0.6 μM, thus the amount of bound V-carbaozle molecules hardly increases. Therefore, should it be necessary to extend the dynamic range on the high end, V-cabazole concentration can be increased.

3) DEPENDENCY OF DYNAMIC RANGE ON ANALYTICAL SIGNAL

Based on the turn-on effect, both the fluorescence lifetime and intensity increase with DNA concentration. Therefore, either the intensity (being the traditionally typical choice) or the lifetime can serve as the analytical signal. In order to select between intensity and lifetime as the analytical signal for DNA detection, the emission spectra measurement is also conducted on a spectrofluorometer (Fluormax-4). The fluorescence spectra across different DNA concentrations are shown in FIGURE 9 (a). As can be reasonably expected, the fluorescence intensity response has a similar trend with

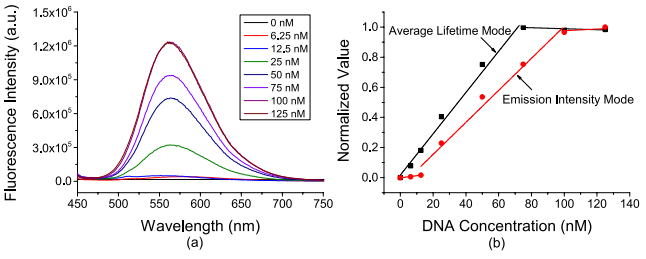

FIGURE 9. (a) Fluorescence intensity across DNA concentrations. (b) Sensor calibration curve based on normalized average lifetime and intensity peaks. Both lifetime- and intensity-mediated DNA detection have similar dynamic range. But lifetime mode has a lower detection limit.

TABLE 2. Comparison of the detection limit of this work with those reported in the literatures for DNA detection.

Probe name[a]	Linear Range (nM)	Detection Limit (nM)	Refs
Conjugated poly (pyridinium salt)	0~60000	1200	[49]
RD2	-	450	[47]
TGA-CdTe/CdS QDs-daunorubicin systems	1380~28000	410	[50]
GO-Ru hybrid	0~70000	33	[51]
GSH-CdTe QDs-praseodymium (III)–rutin complex systems	87.4~20000	26.2	[52]
Cysteine-capped ZnS nanoparticles	100~600	24.6	[53]
Ethidium Bromide	-	20	[54]
9-Anthracenecarboxylic acid-CTMAB	80~1000	19	[55]
Graphene/DNA-CdTe QDs	50~1600	10.4	[56]
Sm^{3+}-modulated GSH-capped CdTe QDs	12~1400	3.61	[57]
DNA-Ag NCs	250~2500	3.57	[1]
AuNPs/DNA/AgNCs	5~100	2.5	[58]
V-carbazole	0~75	1.38	This work
CdTe–CDs–MTX	0~50	1	[59]
AgNCs-DNA	0~200	0.297	[60]
SiNDs/Cy5-c27a	0~20	0.16	[61]
Graphene Nanoprobe	0~25	0.1	[62]
SiNPs	0.01~1	0.0025	[63]
AgNCs/DNA/AuNPs	0.0001~0.001	0.0000334	[64]

[a] The probe name used in the literature.

respect to the average lifetime, but with a shifted dynamic range, as shown in FIGURE 9 (b).

Evidently, using the lifetime as the analytical signal provides a lower detection limit, i.e. is more suitable for the detection of lower DNA concentrations than using the intensity. As evident in FIGURE 9 (b), when the DNA concentration is at 12.5 nM, the average lifetime increases approximately 20%, whereas the intensity is almost unchanged. The opposite is true at a target concentration of 75 nM, where the lifetime becomes insensitive. In addition, it is evident from the emission spectra that, with an increase in DNA concentration, the intensity peaks shift slightly towards shorter wavelengths. The reason is that the energy gap of V-carbazole molecule increases upon binding to DNA, as depicted in FIGURE 2 (d). Therefore, intensity

and lifetime analyses are complementary methods that can be chosen according to application requirement.

4) DETECTION LIMIT

As demonstrated in the FIGURE 8 (d), a linear calibration plot of fluorescence average lifetime against DNA concentration is obtained in the range of 0 to 75 nM with a correlation coefficient of 0.993 and a linear regression equation, as given by

$$\tau_{av} = 0.068 \times C + 1.15 \tag{5}$$

where C is DNA concentration in nM. A detection limit of 1.38 nM for DNA is estimated by using 3 σ /S. S is the slope of the calibration plot and σ is the standard deviation of intercept. Both S and σ are obtained by linear fitting [48]. As shown in TABLE 2, although, the detection limit of our work is moderate compared to the biosensors utilizing amplification methods to provide satisfied detection limit, the detection limit of our work is superior or comparable to those of the existing amplification-free biosensor for DNA detection. In addition, it should be pointed out that the proposed bioassay is simple, non-toxic, suitable for biological applications and the proposed compact, cost-effective LCW DNA biosensor is capable of determining the concentration DNA quantitatively and accurately.

V. CONCLUSION

This work presents a fully-integrated DNA biosensor based on liquid-core waveguide (LCW) optics and TCSPC electronics for fluorescence lifetime analysis. The DNA biosensor encompasses all-custom bioassay, optics and electronics into a microsystem, overcoming the well-known challenge of bulky and expensive hardware requirements for TCSPC, which had prohibited their use in portable and point-of-care applications. The V-carbazole probe is exploited as a lifetime probe in DNA detection for the first time. Excitation propagation within the LCW is investigated both analytically and in simulations, enabling the LCW to deliver superior performance in emission filtering and lifetime measurement accuracy via minimization of temporal dispersion. Prototype characterization has shown detection of DNA down to 15 base pairs at a low detection limit of 1.38 nM. A differential analysis against its commercial bench-top counterpart demonstrates that the proposed biosensor achieves comparable performance, but at a fraction of the system size and component count. The proposed technique elucidates a design approach for compact, application-specific, and low-cost diagnostics biosensor devices.

REFERENCES

[1] D. Han and C. Wei, "Nucleic acid probe based on DNA-templated silver nanoclusters for turn-on fluorescence detection of tumor suppressor gene p53," *RSC Adv.*, vol. 8, no. 45, pp. 25611–25616, Jul. 2018.

[2] S. Arun, A. Shivalingam, M. A. Izquierdo, A. Le Marois, A. Vyšniauskas, K. Suhling, M. K. Kuimova, and R. Vilar, "The interactions between a small molecule and G-quadruplexes are visualized by fluorescence lifetime imaging microscopy," *Nature Commun.*, vol. 6, Sep. 2015, Art. no. 8178.

[3] J. Xu and C. Wei, "The aptamer DNA-templated fluorescence silver nanoclusters: ATP detection and preliminary mechanism investigation," *Biosensors Bioelectron.*, vol. 87, pp. 422–427, Jan. 2017.

[4] Z. Dai, H. M. Leung, and P. K. Lo, "Stimuli-responsive self-assembled DNA nanomaterials for biomedical applications," *Small*, vol. 13, no. 7, 2017, Art. no. 1602881.

[5] J. de Vries, S. Schnichels, J. Hurst, L. Strudel, A. Gruszka, M. Kwak, K.-U. Bartz-Schmidt, M. S. Spitzer, and A. Herrmann, "DNA nanoparticles for ophthalmic drug delivery," *Biomaterials*, vol. 157, pp. 98–106, Mar. 2018.

[6] D. R. G. Pitter, J. Wigenius, A. S. Brown, J. D. Baker, F. Westerlund, and J. N. Wilson, "Turn-on, fluorescent nuclear stains with live cell compatibility," *Org. Lett.*, vol. 15, no. 6, pp. 1330–1333, Mar. 2013.

[7] M. S. Chan, D. Y. Tam, Z. Dai, L. S. Liu, J. W.-T. Ho, M. L. Chan, D. Xu, M. S. Wong, C. Tin, and P. K. Lo, "Mitochondrial delivery of therapeutic agents by amphiphilic DNA nanocarriers," *Small*, vol. 12, no. 6, pp. 770–781, Feb. 2016.

[8] J. R. Lakowicz, *Principles of Fluorescence Spectroscopy*. New York, NY, USA: Springer, 2007.

[9] R. M. Field, S. Realov, and K. L. Shepard, "A 100 fps, time-correlated single-photon-counting-based fluorescence-lifetime imager in 130 nm CMOS," *IEEE J. Solid-State Circuits*, vol. 49, no. 4, pp. 867–880, Apr. 2014.

[10] M.-W. Seo, K. Kagawa, K. Yasutomi, Y. Kawata, N. Teranishi, Z. Li, and I. A. Halin, "A 10 ps time-resolution CMOS image sensor with two-tap true-CDS lock-in pixels for fluorescence lifetime imaging," *IEEE J. Solid-State Circuits*, vol. 51, no. 1, pp. 141–154, Jan. 2016.

[11] F. Villa, R. Lussana, D. Tamborini, A. Tosi, and F. Zappa, "High-fill-factor 60×1 SPAD array with 60 subnanosecond integrated TDCs," *IEEE Photon. Technol. Lett.*, vol. 27, no. 12, pp. 1261–1264, 2015.

[12] D. Ho, M. O. Noor, U. J. Krull, G. Gulak, and R. Genov, "CMOS spectrally-multiplexed FRET-on-a-chip for DNA analysis," *IEEE Trans. Biomed. Circuits Syst.*, vol. 7, no. 5, pp. 643–654, Oct. 2013.

[13] J. Lim, P. Gruner, M. Konrad, and J.-C. Baret, "Micro-optical lens array for fluorescence detection in droplet-based microfluidics," *Lab Chip*, vol. 13, no. 8, pp. 1472–1475, Jan. 2013.

[14] P. Novo, V. Chu, and J. P. Conde, "Integrated fluorescence detection of labeled biomolecules using a prism-like PDMS microfluidic chip and lateral light excitation," *Lab Chip*, vol. 14, no. 12, pp. 1991–1995, Apr. 2014.

[15] J. Koh, J. Kim, J. H. Shin, and W. Lee, "Fabrication and integration of microprism mirrors for high-speed three-dimensional measurement in inertial microfluidic system," *Appl. Phys. Lett.*, vol. 105, no. 11, 2014, Art. no. 114103.

[16] L. Shen, M. Ratterman, D. Klotzkin, and I. Papautsky, "A CMOS optical detection system for point-of-use luminescent oxygen sensing," *Sens. Actuators B, Chem.*, vol. 155, no. 1, pp. 430–435, 2011.

[17] M. A. Stott, V. Ganjalizadeh, M. H. Olsen, M. Orfila, J. McMurray, H. Schmidt, and A. R. Hawkins, "Optimized ARROW-based MMI waveguides for high fidelity excitation patterns for optofluidic multiplexing," *IEEE J. Quantum Electron.*, vol. 54, no. 3, Jun. 2018, Art. no. 6200107.

[18] T. Yang, S. Stavrakis, and A. de Mello, "A high-sensitivity, integrated absorbance and fluorescence detection scheme for probing picoliter-volume droplets in segmented flows," *Anal. Chem.*, vol. 89, no. 23, pp. 12880–12887, Nov. 2017.

[19] A. Allouch, M. Guglielmino, C. A. Serra, and S. Le Calvé, "Optofluidic fluorescence cell for the detection of low concentration toxic gases," *Sens. Actuators B, Chem.*, vol. 255, pp. 3441–3446, Feb. 2018.

[20] H. Cai, J. W. Parks, T. A. Wall, M. A. Stott, A. Stambaugh, K. Alfson, A. Griffiths, R. A. Mathies, R. Carrion, J. L. Patterson, A. R. Hawkins, and H. Schmidt, "Optofluidic analysis system for amplification-free, direct detection of Ebola infection," *Sci. Rep.*, vol. 5, Sep. 2015, Art. no. 14494.

[21] S.-K. Fan, H.-P. Lee, C.-C. Chien, Y.-W. Lu, Y. Chiu, and F.-Y. Lin, "Reconfigurable liquid-core/liquid-cladding optical waveguides with dielectrophoresis-driven virtual microchannels on an electromicrofluidic platform," *Lab Chip*, vol. 16, no. 5, pp. 847–854, 2016.

[22] G. Persichetti, I. A. Grimaldi, G. Testa, and R. Bernini, "Multifunctional optofluidic lab-on-chip platform for Raman and fluorescence spectroscopic microfluidic analysis," *Lab Chip*, vol. 17, no. 15, pp. 2631–2639, Aug. 2017.

[23] M. Guglielmino, P. Bernhardt, C. Trocquet, C. A. Serra, and S. Le Calvé, "On-line gaseous formaldehyde detection by a microfluidic analytical method based on simultaneous uptake and derivatization in a temperature controlled annular flow," *Talanta*, vol. 172, pp. 102–108, Sep. 2017.

[24] K. Du, H. Cai, M. Park, T. A. Wall, M. A. Stott, K. J. Alfson, A. Griffiths, R. Carrion, J. L. Patterson, A. R. Hawkins, H. Schmidt, and R. A. Mathies, "Multiplexed efficient on-chip sample preparation and sensitive amplification-free detection of Ebola virus," *Biosensors Bioelectron.*, vol. 91, pp. 489–496, May 2017.

[25] D. Ozcelik, J. W. Parks, T. A. Wall, M. A. Stott, H. Cai, J. W. Parks, A. R. Hawkins, and H. Schmidt, "Optofluidic wavelength division multiplexing for single-virus detection," *Proc. Nat. Acad. Sci. USA*, vol. 112, no. 42, pp. 12933–12937, 2015.

[26] A. Liebert, H. Wabnitz, D. Grosenick, and R. Macdonald, "Fiber dispersion in time domain measurements compromising the accuracy of determination of optical properties of strongly scattering media," *J. Biomed. Opt.*, vol. 8, no. 3, pp. 512–517, Jul. 2003.

[27] X. J. Feng, P. L. Wu, F. Bolze, H. W. C. Leung, K. F. Li, N. K. Mak, D. W. J. Kwong, J.-F. Nicoud, K. W. Cheah, and M. S. Wong, "Cyanines as new fluorescent probes for dna detection and two-photon excited bioimaging," *Org. Lett.*, vol. 12, no. 10, pp. 2194–2197, May 2010.

[28] S. Sasaki, G. P. C. Drummen, and G.-C. Konishi, "Recent advances in twisted intramolecular charge transfer (TICT) fluorescence and related phenomena in materials chemistry," *J. Mater. Chem. C*, vol. 4, no. 14, pp. 2731–2743, Mar. 2016.

[29] C. Zhong, "The driving forces for twisted or planar intramolecular charge transfer," *Phys. Chem. Chem. Phys.*, vol. 17, no. 14, pp. 9248–9257, Mar. 2015.

[30] L. Wei, Y. Tian, W. Yan, K. Cheung, and D. Ho, "Liquid-core waveguide TCSPC sensor for high-accuracy fluorescence lifetime analysis," *Anal. Bioanal. Chem.*, vol. 411, no. 16, pp. 3641–3652, 2019.

[31] W. Becker, *Advanced Time-Correlated Single Photon Counting Techniques*. Berlin, Germany: Springer, 2005.

[32] W. Liping, Y. Wenrong, T. Yi, and H. Derek, "Model of TCSPC fluorescence lifetime analysis microsystem using Monte Carlo methods," presented at the IEEE Int. Conf. Electron Devices Solid-State Circuits (EDSSC), Hong Kong, 2016.

[33] A. Cuccato, S. Antonioli, M. Crotti, I. Labanca, A. Gulinatti, I. Rech, and M. Ghioni, "Complete and compact 32-channel system for time-correlated single-photon counting measurements," *IEEE Photon. J.*, vol. 5, no. 5, Oct. 2013, Art. no. 6801514.

[34] Y. Tian, W. Yan, L. Wei, and D. Ho, "Low detection limit time-correlated single photon counting lifetime analytical system for point-of-care applications," *IEEE Access*, vol. 7, pp. 18256–18266, 2019.

[35] T. Robinson, P. Valluri, G. Kennedy, A. Sardini, C. Dunsby, M. A. A. Neil, G. S. Baldwin, P. M. W. French, and A. J. de Mello, "Analysis of DNA binding and nucleotide flipping kinetics using two-color two-photon fluorescence lifetime imaging microscopy," *Anal. Chem.*, vol. 86, no. 21, pp. 10732–10740, Sep. 2014.

[36] T. Niehörster, A. Löschberger, I. Gregor, B. Krämer, H.-J. Rahn, M. Patting, F. Koberling, J. Enderlein, and M. Sauer, "Multi-target spectrally resolved fluorescence lifetime imaging microscopy," *Nature Methods*, vol. 13, no. 3, pp. 257–262, Jan. 2016.

[37] R. Gill, I. Willner, I. Shweky, and U. Banin, "Fluorescence resonance energy transfer in CdSe/ZnS-DNA conjugates: Probing hybridization and DNA cleavage," *J. Phys. Chem. B*, vol. 109, no. 49, pp. 23715–23719, Nov. 2005.

[38] N. Ehrlich, K. Anhalt, H. Paulsen, S. Brakmann, and C. G. Hübner, "Exonucleolytic degradation of high-density labeled DNA studied by fluorescence correlation spectroscopy," *Analyst*, vol. 137, no. 5, pp. 1160–1167, Jan. 2012.

[39] N.-T. Chen, C.-Y. Wu, C.-Y. Chung, Y. Hwu, S.-H. Cheng, C.-Y. Mou, and L.-W. Lo, "Probing the dynamics of doxorubicin-DNA intercalation during the initial activation of apoptosis by fluorescence lifetime imaging microscopy (FLIM)," *PLoS One*, vol. 7, no. 9, Sep. 2012, Art. no. e44947.

[40] B. J. Harvey, C. Perez, and M. Levitus, "DNA sequence-dependent enhancement of Cy3 fluorescence," *Photochem. Photobiol. Sci.*, vol. 8, no. 8, pp. 1105–1110, Jun. 2009.

[41] J. Shi, M. Zhou, A. Gong, Q. Li, Q. Wu, G. J. Cheng, M. Yang, and Y. Sun, "Fluorescence lifetime imaging of nanoflares for mRNA detection in living cells," *Anal. Chem.*, vol. 88, no. 4, pp. 1979–1983, Jan. 2016.

[42] M. Sholokh, O. M. Zamotaiev, R. Das, V. Y. Postupalenko, L. Richert, D. Dujardin, O. A. Zaporozhets, V. G. Pivovarenko, A. S. Klymchenko, and Y. Mély, "Fluorescent amino acid undergoing excited state intramolecular proton transfer for site-specific probing and imaging of peptide interactions," *J. Phys. Chem. B*, vol. 119, no. 6, pp. 2585–2595, Oct. 2014.

[43] M. E. Sanborn, B. K. Connolly, K. Gurunathan, and M. Levitus, "Fluorescence properties and photophysics of the sulfoindocyanine Cy3 linked covalently to DNA," *J. Phys. Chem. B*, vol. 111, no. 37, pp. 11064–11074, Aug. 2007.

[44] P.-J. J. Huang and J. Liu, "DNA-length-dependent fluorescence signaling on graphene oxide surface," *Small*, vol. 8, no. 7, pp. 977–983, Apr. 2012.

[45] D. Dziuba, P. Jurkiewicz, M. Cebecauer, M. Hof, and M. Hocek, "A rotational BODIPY nucleotide: An environment-sensitive fluorescence-lifetime probe for DNA interactions and applications in live-cell microscopy," *Angew. Chem. Int. Ed.*, vol. 128, no. 1, pp. 182–186, Jan. 2016.

[46] R. K. P. Benninger, O. Hofmann, B. Önfelt, I. Munro, C. Dunsby, D. M. Davis, M. A. A. Neil, P. M. W. French, and A. J. de Mello, "Fluorescence-lifetime imaging of DNA–dye interactions within continuous-flow microfluidic systems," *Angew. Chem. Int. Ed.*, vol. 46, no. 13, pp. 2228–2231, 2007.

[47] P. Gaur, A. Kumar, R. Dalal, R. Kumar, S. Bhattacharyya, and S. Ghosh, "Selectivity advancement through chemical structure engineering: Long-term intracellular DNA recognition, chromosomal staining and micronuclei detection," *Sens. Actuators B, Chem.*, vol. 248, pp. 690–698, Sep. 2017.

[48] H. Zhang, R. Liu, Y. Tan, W. H. Xie, H. Lei, H.-Y. Cheung, and H. Sun, "A FRET-based ratiometric fluorescent probe for nitroxyl detection in living cells," *ACS Appl Mater Interfaces*, vol. 7, no. 9, pp. 5438–5443, Feb. 2015.

[49] J. Sun, Y. Lu, L. Wang, D. Cheng, Y. Sun, and X. Zeng, "Fluorescence turn-on detection of DNA based on the aggregation-induced emission of conjugated poly(pyridinium salt)s," *Polym. Chem.*, vol. 4, no. 14, pp. 4045–4051, May 2013.

[50] P. Li, S. Liu, S. Yan, X. Fan, and Y. He, "A sensitive sensor for anthraquinone anticancer drugs and hsDNA based on CdTe/CdS quantum dots fluorescence reversible control," *Colloids Surfaces A, Physicochem. Eng. Aspects*, vol. 392, no. 1, pp. 7–15, Dec. 2011.

[51] H. Li, F. Liu, S. Sun, J. Wang, Z. Li, D. Mu, B. Qiao, and X. Peng, "Interaction of $Ru(phen)_3Cl_2$ with graphene oxide and its application for DNA detection both *in vitro* and *in vivo*," *J. Mater. Chem. B*, vol. 1, no. 33, pp. 4146–4151, 2013.

[52] Z. Liu, S. Liu, X. Wang, P. Li, and Y. He, "A novel quantum dots-based OFF–ON fluorescent biosensor for highly selective and sensitive detection of double-strand DNA," *Sens. Actuators B, Chem.*, vol. 176, pp. 1147–1153, Jan. 2013.

[53] Y. Li, J. Chen, C. Zhu, L. Wang, D. Zhao, S. Zhuo, and Y. Wu, "Preparation and application of cysteine-capped ZnS nanoparticles as fluorescence probe in the determination of nucleic acids," *Spectrochimica Acta A, Mol. Biomol. Spectrosc.*, vol. 60, nos. 8–9, pp. 1719–1724, Jul. 2004.

[54] J. D. Kimball, B. Maliwal, S. L. Raut, H. Doan, Z. Nurekeyev, I. Gryczynskic, and Z. Gryczynski, "Enhanced DNA detection using a multiple pulse pumping scheme with time-gating (MPPTG)," *Analyst*, vol. 143, no. 12, pp. 2819–2827, May 2018.

[55] J. Liu, X. Wang, and L. Wang, "A novel spectrofluorimetric method for the determination of DNA," *Spectrochimica Acta A, Mol. Biomol. Spectrosc.*, vol. 63, no. 1, pp. 32–35, Jan. 2006.

[56] C. Zhang, J. Xu, S. Zhang, X. Ji, and Z. He, "One-pot synthesized DNA–CdTe quantum dots applied in a biosensor for the detection of sequence-specific oligonucleotides," *Chem.-Eur. J.*, vol. 18, no. 27, pp. 8296–8300, 2012.

[57] Y. Shen, S. Liu, J. Yang, L. Wang, X. Tan, and Y. He, "A novel and sensitive turn-on fluorescent biosensor for the DNA detection using Sm^{3+}-modulated glutathione-capped CdTe quantum dots," *Sens. Actuators B, Chem.*, vol. 199, pp. 389–397, Aug. 2014.

[58] J.-L. Ma, B.-C. Yin, H.-N. Le, and B.-C. Ye, "Label-free detection of sequence-specific DNA based on fluorescent silver nanoclusters-assisted surface plasmon-enhanced energy transfer," *ACS Appl. Mater. Interfaces*, vol. 7, no. 23, pp. 12856–12863, May 2015.

[59] S.-S. Liang, L. Qi, R.-L. Zhang, M. Jin, and Z.-Q. Zhang, "Ratiometric fluorescence biosensor based on CdTe quantum and carbon dots for double strand DNA detection," *Sens. Actuators B, Chem.*, vol. 244, pp. 585–590, Jun. 2017.

[60] H. Kim, S. Kang, K. S. Park, and H. G. Park, "Enzyme-free and label-free miRNA detection based on target-triggered catalytic hairpin assembly and fluorescence enhancement of DNA-silver nanoclusters," *Sens. Actuators B, Chem.*, vol. 260, pp. 140–145, May 2018.

[61] Y. Zhang, X. Ning, G. Mao, X. Ji, and Z. He, "Fluorescence turn-on detection of target sequence DNA based on silicon nanodot-mediated quenching," *Anal. Bioanal. Chem.*, vol. 410, pp. 3209–3216, May 2018.
[62] S. He, B. Song, D. Li, C. Zhu, W. Qi, Y. Wen, L. Wang, S. Song, H. Fang, and C. Fan, "A graphene nanoprobe for rapid, sensitive, and multicolor fluorescent DNA analysis," *Adv. Funct. Mater.*, vol. 20, no. 3, pp. 453–459, 2010.
[63] L. Ding, H. Liu, L. Zhang, L. Li, and J. Yu, "Label-free detection of microRNA based on the fluorescence quenching of silicon nanoparticles induced by catalyzed hairpin assembly coupled with hybridization chain reaction," *Sens. Actuators B, Chem.*, vol. 254, pp. 370–376, Jan. 2018.
[64] X. Miao, Z. Cheng, H. Ma, Z. Li, N. Xue, and P. Wang, "Label-free platform for MicroRNA detection based on the fluorescence quenching of positively charged gold nanoparticles to silver nanoclusters," *Anal. Chem.*, vol. 90, no. 2, pp. 1098–1103, Jan. 2018.

LIPING WEI received the B.Sc. degree in electronic science and technology and the M.Sc. degree in technology and instrument of test and measurement from the North University of China, China, in 2011 and 2014, respectively. She is currently pursuing the Ph.D. degree in materials science and engineering with the City University of Hong Kong, Hong Kong. Her research interest includes developing compact time-correlated single photon counting fluorescence lifetime measurement systems for biological sensing applications.

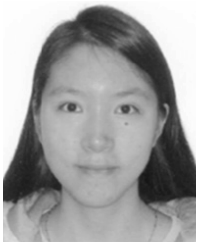

HOI MAN LEUNG received the B.Sc. degree in chemistry from the City University of Hong Kong, Hong Kong, in 2017, where she is currently pursuing the Ph.D. degree. Her research interest includes the development of functional DNA- and nanoparticle-based materials for biomedical application.

YI TIAN received the B.Sc. degree in electronics information science and technology and the M.Sc. degree in circuit and system from Lanzhou University, Lanzhou, China, in 2010 and 2013, respectively. He is currently pursuing the Ph.D. degree in materials science and engineering with the City University of Hong Kong, Hong Kong. His research interest includes the development of compact time-correlated single photon counting lifetime analytical systems.

PIK KWAN LO received the B.Sc. and M.Phil. degrees from Hong Kong Baptist University, in 2004 and 2006, respectively, and the Ph.D. degree from McGill University, Canada, in 2010. She was Postdoctoral Researcher with Harvard University, from 2010 to 2012. She is currently an Associate Professor with the Department of Chemistry, City University of Hong Kong. Her research area is highly interdisciplinary and lies at the interface between chemistry, biology, nanotechnology, and materials science. Her research interest includes developing multifunctional nano-sized materials and applying them for biomedical and technological applications.

DEREK HO received the B.Sc. (Hons.) and M.A.Sc. degrees from the University of British Columbia (UBC), Vancouver, Canada, in 2005 and 2007, respectively, and the Ph.D. degree from the University of Toronto, Toronto, Canada, in 2013, all in electrical and computer engineering. He is currently an Associate Professor with the Department of Materials Science and Engineering, City University of Hong Kong. His research interests include the synthesis of nanostructured materials, device optimization, and microsystem integration for applications in chemical, physical, and biological sensors.